Weak Exciton Scattering in Molecular Nanotubes Revealed by Double-Quantum Two-Dimensional Electronic Spectroscopy

Darius Abramavicius,[1,2] Alexandra Nemeth,[3] Franz Milota,[3] Jaroslaw Sperling,[4] Shaul Mukamel,[5] and Harald F. Kauffmann[3,6,*]

[1]*State Key Laboratory of Supramolecular Structure and Materials, Jilin University, Changchun 130012, China*
[2]*Department of Theoretical Physics, Vilnius University, Saulėtekio al. 9-III, LT-10222 Vilnius, Lithuania*
[3]*Faculty of Physics, University of Vienna, 1090 Vienna, Austria*
[4]*Newport Spectra-Physics, Darmstadt 64291, Germany*
[5]*Department of Chemistry, University of California, Irvine, California 92697-2025, USA*
[6]*Faculty of Physics, Vienna University of Technology, 1040 Vienna, Austria*

(Received 2 September 2011; published 7 February 2012)

The two-exciton manifold of a double-wall cylindrical molecular aggregate is studied using a coherent third order optical technique. Experiments reveal the anharmonic character of the exciton bands. Atomistic simulations of the exciton-exciton scattering show that the excitons can be treated as weakly coupled hard-core bosons. The weak coupling stems from the extended exciton delocalization made possible by the nanotube geometry.

DOI: 10.1103/PhysRevLett.108.067401 PACS numbers: 78.67.Ch, 78.40.Ri, 78.47.nj, 78.67.Sc

The dynamics of interacting excitons manifests in many molecular, semiconductor, and biological systems. Photosynthetic aggregates and DNA are optimized to avoid damage under high levels of irradiation [1,2]. Exciton-exciton annihilation controls dephasing in carbon nanotubes [3] and molecular aggregates [4,5]. Inelastic exciton-exciton interaction is unwelcome in light harvesting antenna, e.g., the chlorosome aggregates designed to store and transfer excitons into energy conversion units [6] since it reduces the quantum yield. Additionally exciton-exciton scattering induces energy shifts. These effects are indirectly observed in the absorption spectrum. More direct observation is possible by pump probe and time-resolved fluorescence techniques [4].

Bound and unbound biexcitons in inorganic semiconductors [7–11], double excitations in molecules [12,13], as well as molecular excitons in photosynthetic molecular aggregates [14,15] have been observed using double-quantum two-dimensional spectroscopy (2Q2D). The 2Q2D spectrum is particularly sensitive to exciton couplings since it vanishes if the contributing excitons do not interact. Strong redshifted peaks are signatures of bound biexcitons, which are strongly correlated exciton pairs. Peaks at the sums of exciton energies indicate weak exciton scattering [14]. This mixed nature of exciton-exciton pairs reflects particle entanglement on the microscopic level [16]. The 2Q2D signal is generated by a sequence of three laser pulses with wave vectors $\mathbf{k}_1$, $\mathbf{k}_2$, and $\mathbf{k}_3$ (in chronological order) in the direction $+\mathbf{k}_1 + \mathbf{k}_2 - \mathbf{k}_3$. In the eigenstate representation the first two pulses (delayed by $t_1 \rightarrow 0$) create a two-exciton coherence [Fig. 1(a)] which is detected by two additional interactions separated by delay t_3. This description can be recast in terms of boson quasiparticles (excitons), which propagate and scatter during the second interval t_2 [7,14,17] [Fig. 1(b)]. The 2Q2D spectrum is displayed by a Fourier transform $t_2 \rightarrow \omega_2$ and $t_3 \rightarrow \omega_3$ which reveals the oscillation frequencies in these intervals.

In this Letter we report the observation of multiexciton effects in a molecular aggregate [3,3'-bis(3-sulfopropyl)-5,5',6,6'-tetrachloro-1,1'-dioctylbenzimidacarbocyanine [C8S3]], which is a synthetic exciton antenna. The compact molecular packing in this aggregate is reminiscent of the chlorosome: the molecular units self-assemble into a long double-wall tubule [18]. The absorption spectrum shown in Fig. 1(c) contains three main peaks e_1, e_2, e_3, in increasing energy. These have been previously ascribed to a longitudinal inner-wall exciton, a longitudinal outer-wall exciton and a mixed feature, respectively [19]. The exciton dynamics in this system has been studied recently [19,20].

The experimental setup has been described in detail elsewhere [13,21]. In short, our apparatus is based on 17 fs laser pulses centered at $\omega_0 = 17\,100\ \mathrm{cm}^{-1}$ [pulse bandwidth FWHM $= 1500\ \mathrm{cm}^{-1}$, shown by dashed line in Fig. 1(c)]. The sequence of four pulses can be manipulated by pairs of movable glass wedges. The phase stability together with the heterodyne detection scheme allow us to recover both amplitude and phase of the signal field.

The experimental 2Q2D spectrum [Fig. 2(a)] shows a set of peaks along $\omega_2 \approx 2\omega_3$ (we denote it as the ''diagonal''), which is marked by a dashed line. Each absorption peak, shown on the right marginal, is associated with a pair of positive and negative peaks in the 2Q2D spectrum, whose splitting is denoted by δ_e. The positive (negative) peaks are redshifted (blueshifted) from the single-exciton energy. This configuration is denoted by $\delta_e > 0$. δ_e grows from $\sim 190\ \mathrm{cm}^{-1}$ for e_1, $\sim 210\ \mathrm{cm}^{-1}$ for e_2, to $\sim 360\ \mathrm{cm}^{-1}$ for e_3 in accord with the absorption peak widths. Several cross

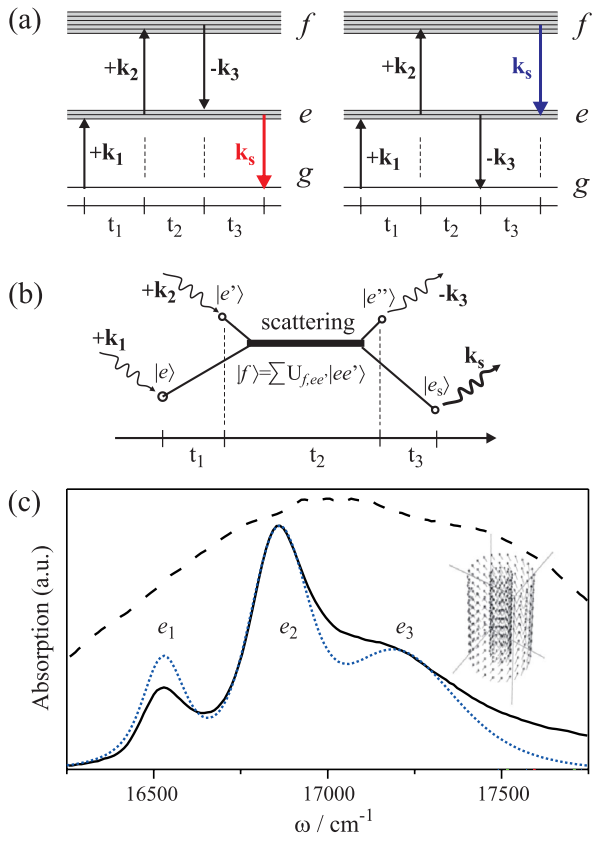

FIG. 1 (color online). (a) 2Q2D measurement viewed as transitions between eigenstates. Time runs from left to right. g, e, and f denote the ground, single and double exciton bands, respectively. (b) Exciton scattering representation of the 2Q2D signal. (c) Experimental (solid black) and simulated (dotted blue) absorption spectrum. The laser power spectrum used in the 2D measurements is shown as black dashed line.

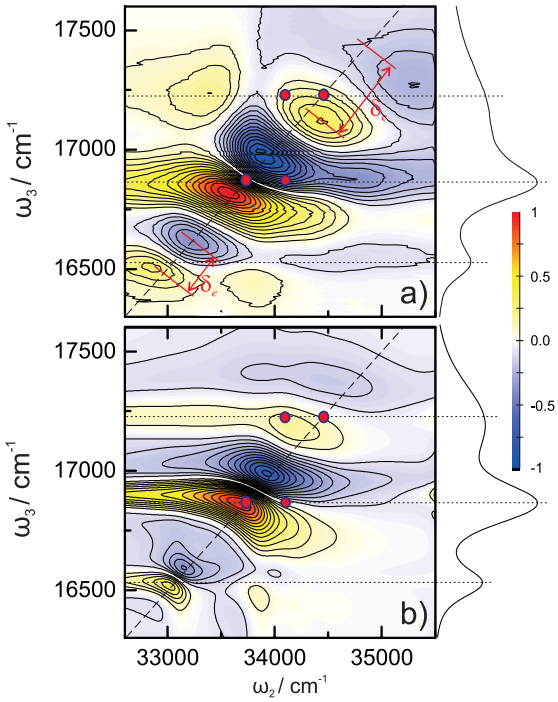

FIG. 2 (color online). (a) Experimental and (b) simulated 2Q2D spectra ($t_1 = 0$) of C8S3 aggregates. Red (blue) contours indicate positive (negative) peaks. Spectra are normalized to their maximum absolute value. Right marginals show the corresponding absorption spectra. Dashed horizontal lines mark the absorption peaks.

peaks appear as shoulders accompanying the diagonal peaks. Those associated with e_1 are weaker than those of e_3. However, due to broad linewidths it is hard to assign the cross peaks directly from the experiment alone.

For a quantitative interpretation of the experiment we have performed microscopic simulations of the exciton scattering process in an infinite one-dimensional double-wall cylindrical aggregate model. We constructed a unit cell of length L with two "walls" [inset in Fig. 1(c)] as follows. Each wall υ (inner or outer) comprises N_υ equally spaced rings (diameter d_υ) repeated along the cylinder axis and contains K_υ equally spaced chromophores within each ring. Each ring is rotated along the cylinder axis with respect to the previous one by an angle θ_υ. The chromophore orientation is defined by the orientation unit vector $\boldsymbol{\mu}$, which for each site is rotated depending on the position in the cell. The reference dipole $\boldsymbol{\mu}_{0\upsilon}$ is chosen at position $(x = d_\upsilon/2, y = 0, z = 0)$, z being the cylinder axis.

The electronic excitations are described using the Frenkel exciton model [22]. The chromophore excitation energy is E_0. Intermolecular coupling was calculated by assuming two charges ($q = \pm 0.34$ e) per site separated by 0.7 nm along $\boldsymbol{\mu}$ [18]. Intercell couplings were truncated at 30 repeat units. Optical transition dipoles are taken along $\boldsymbol{\mu}$ as well. The dephasing rate was evaluated using a fluctuating Brownian oscillator model, coupled to each chromophore, and characterized by a time scale of 50 fs and a strength of 500 cm^{-1} [19]. Inhomogeneous broadening in all signals was incorporated by convoluting the homogeneous spectra with a Gaussian function [23] whose variance in the 16 000–18 000 cm^{-1} interval depends on frequency as $\sigma_0 \exp[(\omega - 14\,700)/526.32]$, here $\sigma_0 = 1$ cm^{-1}.

Periodic boundary conditions along the cylinder axis give Bloch-type exciton states with a lattice wave vector κ. Since the optical wavelength is much larger than the typical exciton coherence size, only excitons with $\kappa \to 0$ are optically active. Selection rules which follow from the cylindrical symmetry imply that only six transitions are bright in an infinite double-wall aggregate (two longitudinal and four pairwise energy-degenerate transverse, resulting in four resonant frequencies). By fitting the geometry and orientations of the site dipoles we reproduced the experimental absorption spectrum shown in Fig. 1(c) ($E_0 = 18\,840$ cm^{-1}, other parameters are summarized in Table I). The longitudinal transitions of the inner and outer cylinder are labeled e_1 and e_2, respectively, and a

TABLE I. Parameters for the C8S3 nanotube with cell length $L = 1.17$ nm.

wall (v)	N	d [Å]	K	θ [deg]	$\boldsymbol{\mu}_0(x, y, z)$
inner	20	10.8	2	9	(0, 0.72, 0.69)
outer	18	15.6	4	5	(0, 0.59, 0.81)

transversal transition stemming from both walls is labeled e_3. The fourth very weak transition, marked e_4 in Fig. 3(a) right marginal, lies between e_1 and e_2.

The 2Q2D signal is induced by the exciton scattering due to the on-site binding energy Δ (two excitations on a chromophore have energy $2E_0 + \Delta$) [14,24]. The homogeneous signal is then given in terms of single-exciton eigenstates with energies ε_e and transition dipoles d_e at $\kappa = 0$, and the exciton scattering matrix Γ [22]:

$$S_h(\omega_3, \omega_2) = \Im \sum_{ijkl} \frac{\langle d_l d_k d_j d_i \rangle}{(\omega_3 - \xi_l)(\omega_2 - \omega_3 - \xi_k^*)} \times \left[\frac{\Gamma_{lk,ji}(\omega_3 + \xi_k^*)}{\omega_3 + \xi_k^* - \xi_i - \xi_j} - \frac{\Gamma_{lk,ji}(\omega_2)}{\omega_2 - \xi_i - \xi_j} \right], \quad (1)$$

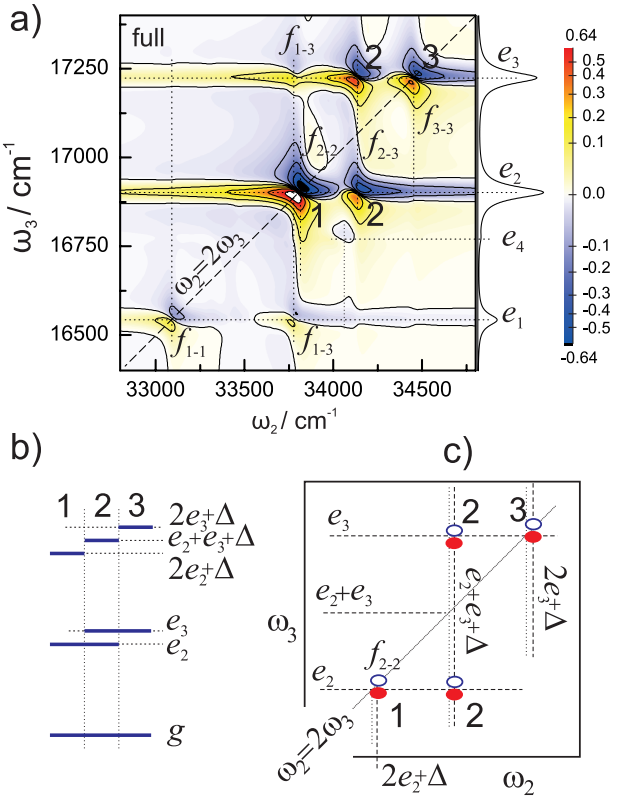

FIG. 3 (color online). (a) Simulated high-resolution (homogeneous) 2Q2D spectrum. The absorption spectrum is shown in the right marginal. Dashed horizontal lines mark the peak maxima, vertical lines mark the sums of single-exciton energies f_{i-j}. (b) Level scheme and (c) the spectum structure of peaks 1–3.

where $ijkl$ runs over e_1-e_3, $\langle d_l d_k d_j d_i \rangle$ is the orientationally averaged product of their transition dipoles, $\xi_j = \varepsilon_j - i\gamma_j$, where γ_j is the dephasing rate of exciton j. $\Gamma_{lk,ji}$ can be numerically calculated for a periodic system as described in Appendix F of Ref. [22]. It is a nonlinear function of Δ. When $|\Delta| < E_0$ we have the soft-core boson model, where two excitations are allowed to occupy the same site. For $\Delta \gg E_0$ we obtain the hard-core model where excitations cannot occupy the same site (two-level sites). The 2Q2D spectrum calculated using the hard-core model (all other parameters are the same as in absorption) shows good overall agreement with the experiment [Fig. 2(b)]. The peak positions, relative intensities, and peak splittings δ_e are reproduced.

The doublet structure along the diagonal is reminiscent of the 2Q2D spectrum of weakly anharmonic vibrations [25]. In order to assign the underlying transitions we plot the homogeneous 2Q2D spectrum [Fig. 3(a)], obtained by setting the dephasing $\gamma = 20$ cm^{-1}. We find that all features are double peaks. Also δ_e in Fig. 2(a) shows the spectral broadening alone. Doublet features can be attributed to overtones of anharmonic exciton oscillators, which we label f_{1-1}-f_{3-3}. The anharmonicity is much smaller than the peak linewidth. Thus, the exciton bands are typical for weakly anharmonic oscillators. The cross peaks reflect their combinations. For three main exciton bands (e_1, e_2, e_3) there are three possible combinations: $f_{1-2} \rightleftharpoons e_1 + e_2$, $f_{1-3} \rightleftharpoons e_1 + e_3$, $f_{2-3} \rightleftharpoons e_2 + e_3$. We clearly identify pairs of cross peaks above and below the diagonal corresponding to f_{2-3} with the energy ω_2 approximately equal to the sum of $e_2 + e_3$. Weaker cross peaks also signify f_{1-3}.

The strongest features are from e_2 and e_3 excitons. Their 2Q2D spectrum can be described by the level scheme of two weakly correlated anharmonic oscillators shown in Figs. 3(b) and 3(c). Their main resonances are ε_{e_2} and ε_{e_3} [e_j in Figs. 3(b) and 3(c)]. Their overtone energies are $\varepsilon_{f_{2-2}} = 2\varepsilon_{e_2} + \Delta$ and $\varepsilon_{f_{3-3}} = 2\varepsilon_{e_3} + \Delta$. There is one mixed configuration $\varepsilon_{f_{2-3}} = \varepsilon_{e_2} + \varepsilon_{e_3} + \Delta$. For $\Delta > 0$ all possible transition configurations can be obtained from Fig. 1(a). The structure of the spectrum when $\Delta \to 0$ is shown in Fig. 3(c). Peaks 1, 2, 3 are marked in the simulated spectrum [Fig. 3(a) as well as Figs. 2(a) and 2(b)]. The similarity between Figs. 3(a) and 3(c) shows that the excitons have small anharmonicity.

When the binding energy vanishes, i.e., $\Delta \to 0$, the scattering matrix is given by [14]

$$\Gamma^{\mathrm{MFA}}_{lk,ji}(\omega) = -i\Delta \sum_m \psi_{ml}\psi_{mk}\psi_{mj}\psi_{mi}, \quad (2)$$

where m labels different sites inside the unit cell, ψ_{mi} is the wave function in site representation of zero-lattice-vector ($\kappa = 0$) exciton e_i (these are real at $\kappa = 0$). We denote this the mean field (MF) approximation. Calculations of the 2Q2D spectrum using Eq. (2) and $\Delta > 0$ (not shown) have

recovered the result of the full hard-core model as described below Eq. (1) with $\Delta \to \infty$.

The similarity between the hard-core and the MF boson model seems surprising since the intermolecular interactions are strong and each molecule acts as a two-level system (two excitations cannot reside on the same site due to Pauli exclusion). This would suggest strong exciton-exciton correlations as was seen in a photosynthetic Fenna-Matthews-Olson (FMO) complex, where the double excitations are composed of various exciton pairs [15] and the MF approximation does not apply [14]. The strong intermolecular interactions in the nanotube result in large exciton delocalization [19]. This is the main reason for weak exciton scattering: delocalized excitons can easily penetrate each other. Another property that supports weak scattering is the positive binding energy Δ. When $\Delta > 0$ the energy of two interacting excitons is higher than the sum of their energies (exciton repulsion). $\Delta < 0$ would have implied exciton attraction. Note that the hard-core model with $\Delta \to \infty$ does not depend on the sign of Δ, while Eq. (2) with $\Delta < 0$ reverses the sign of the scattering matrix.

If the exciton scattering amplitude depends on exciton delocalization, a strong dependence on the diagonal disorder is expected. Strong scattering would lead to strong cross peaks in 2Q2D spectra. However, the weak scattering limit seems to apply even for the broadest peak e_3. Further simulations with the disorder included microscopically would be useful to verify this effect. Because of the weak scattering, the double resonance can be assigned to a given exciton pair, which correlates their wave functions [16]. Our experiment thus provides the first evidence for pairwise exciton-exciton entanglements.

The exciton configurations f_{i-j} can be associated with the system geometry. Note that e_1 (e_2) is the exciton band of the inner (outer) tube. The spectral properties of f_{1-1} characterize exciton scattering inside the inner tube, f_{2-2}—inside the outer tube, while f_{1-2} reveals intertube scattering. Since f_{1-1} is much weaker than f_{2-2} in Fig. 3(a), the intrascattering of the outer excitons is stronger than that of the inner excitons. Since f_{1-2} is weak as well the inner excitons are the most independent particles. Note that the e_3 band excitons are delocalized in both tubes. Figure 3(a) shows that the outer e_2 excitons scatter not only between themselves but also with e_3 excitons as observed from strong f_{2-3} features. This result depends on the nanotube packing (the interwall distance). The dipole-dipole coupling depends on the distance as R^{-3}. Thus for large interwall distances the walls become independent and the interwall exciton scattering would decay. However, this should not affect the intrawall scattering.

In conclusion, we have observed a weak exciton-exciton scattering process in a molecular nanotube. The strong Pauli exclusion is diluted due to exciton delocalization. This property may be useful for exciton antenna applications since exciton repulsion and weak scattering are expected to reduce exciton annihilation.

D. A. acknowledges support of Research Council of Lithuania Grant No. VP1-3.1-ŠMM-07-K-01-020. S. M. acknowledges the support of the National Science Foundation (Grant No. CHE-1058791), DARPA BAA-10-40 QuBE, and the Chemical Sciences, Geosciences and Biosciences Division, Office of Basic Energy Sciences, Office of Science, U.S. Department of Energy. A. N. and J. S. thank the Austrian Academy of Sciences (ÖAW) and F. M. thanks the Austrian Science Foundation (FWF) for financial support.

*harald.f.kauffmann@univie.ac.at

[1] A. V. Ruban, R. Berera, C. Ilioaia, I. H. M. van Stokkum, J. T. M. Kennis, A. A. Pascal, H. van Amerongen, B. Robert, P. Horton, and R. van Grondelle, Nature (London) **450**, 575 (2007).
[2] I. Buchvarov, Q. Wang, M. Raytchev, A. Trifonov, and T. Fiebig, Proc. Natl. Acad. Sci. U.S.A. **104**, 4794 (2007).
[3] D. Abramavicius, Y.-Z. Ma, M. W. Graham, L. Valkunas, and G. R. Fleming, Phys. Rev. B **79**, 195445 (2009).
[4] G. Trinkunas, J. L. Herek, T. Polívka, V. Sundström, and T. Pullerits, Phys. Rev. Lett. **86**, 4167 (2001).
[5] B. Brüggemann and T. Pullerits, New J. Phys. **13**, 025024 (2011).
[6] G. T. Oostergetel, H. van Amerongen, and E. J. Boekema, Photosynth. Res. **104**, 245 (2010).
[7] L. Yang and S. Mukamel, Phys. Rev. Lett. **100**, 057402 (2008).
[8] D. B. Turner and K. A. Nelson, Nature (London) **466**, 1089 (2010).
[9] K. W. Stone, K. Gundogdu, D. B. Turner, X. Li, S. T. Cundiff, and K. A. Nelson, Science **324**, 1169 (2009).
[10] D. Karaiskaj, A. D. Bristow, L. Yang, X. Dai, R. P. Mirin, S. Mukamel, and S. T. Cundiff, Phys. Rev. Lett. **104**, 117401 (2010).
[11] R. P. Smith, J. K. Wahlstrand, A. C. Funk, R. P. Mirin, S. T. Cundiff, J. T. Steiner, M. Schafer, M. Kira, and S. W. Koch, Phys. Rev. Lett. **104**, 247401 (2010).
[12] J. Kim, V. M. Huxter, C. Curutchet, and G. D. Scholes, J. Phys. Chem. A **113**, 12122 (2009).
[13] A. Nemeth, F. Milota, T. Mancal, T. Pullerits, J. Sperling, J. Hauer, H. F. Kauffmann, and N. Christensson, J. Chem. Phys. **133**, 094505 (2010).
[14] D. Abramavicius, D. V. Voronine, and S. Mukamel, Proc. Natl. Acad. Sci. U.S.A. **105**, 8525 (2008).
[15] J. M. Dawlaty, D. I. G. Bennett, V. M. Huxter, and G. R. Fleming, J. Chem. Phys. **135**, 044201 (2011).
[16] S. Mukamel, J. Chem. Phys. **132**, 241105 (2010).
[17] S. Mukamel, R. Oszwaldowski, and D. Abramavicius, Phys. Rev. B **75**, 245305 (2007).

[18] C. Didraga, A. Pugzlys, P. R. Hania, H. von Berlepsch, K. Duppen, and J. Knoester, J. Phys. Chem. B **108**, 14976 (2004).
[19] J. Sperling, A. Nemeth, J. Hauer, D. Abramavicius, S. Mukamel, H. F. Kauffmann, and F. Milota, J. Phys. Chem. A **114**, 8179 (2010).
[20] J. M. Womick, S. A. Miller, and A. M. Moran, J. Phys. Chem. A **113**, 6587 (2009).
[21] A. Nemeth, J. Sperling, J. Hauer, H. F. Kauffmann, and F. Milota, Opt. Lett. **34**, 3301 (2009).
[22] D. Abramavicius and S. Mukamel, Chem. Phys. **318**, 50 (2005).
[23] D. Abramavicius and S. Mukamel, J. Chem. Phys. **134**, 174504 (2011).
[24] V. Chernyak, W. M. Zhang, and S. Mukamel, J. Chem. Phys. **109**, 9587 (1998).
[25] E. C. Fulmer, P. Mukherjee, A. T. Krummel, and M. T. Zanni, J. Chem. Phys. **120**, 8067 (2004).